# Phase-Selective Cation-Exchange Chemistry in Sulfide Nanowire Systems

**Dandan Zhang†[§], Andrew B. Wong†[§], Yi Yu†[§], Sarah Brittman†[§], Jianwei Sun†[§], Anthony Fu†[§], Brandon Beberwyck‡[§∥], A. Paul Alivisatos†‡[§∥], and Peidong Yang*†‡[§∥]**

[†]Department of Chemistry, [‡]Department of Materials Science and Engineering, University of California, Berkeley, California 94720, United States

[§] Materials Sciences Division, Lawrence Berkeley National Laboratory, Berkeley, California 94720, United States

[∥] Kavli Energy Nanoscience Institute, Berkeley, California 94720, United States

**DOI:** 10.1021/ja511010q

p_yang@berkeley.edu

•

## Abstract

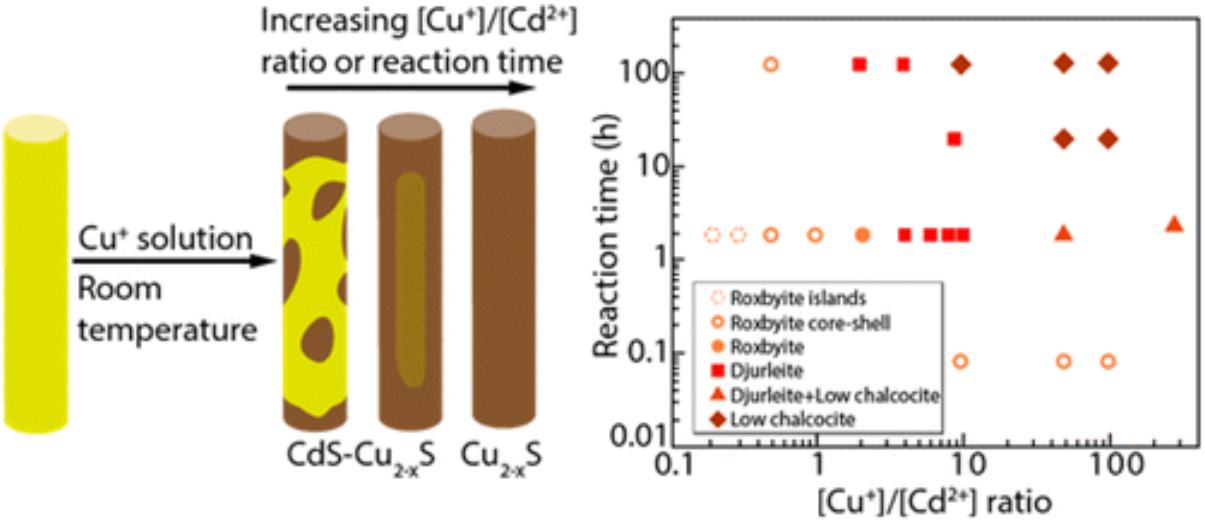


As a cation-deficient, *p*-type semiconductor, copper sulfide ($Cu_{2-x}S$) shows promise for applications such as photovoltaics, memristors, and plasmonics. However, these applications demand precise tuning of the crystal phase as well as the stoichiometry of $Cu_{2-x}S$, an ongoing challenge in the synthesis of $Cu_{2-x}S$ materials for a specific application. Here, a detailed transformation diagram of cation-exchange (CE) chemistry from cadmium sulfide (CdS) into $Cu_{2-x}S$ nanowires (NWs) is reported. By varying the reaction time and the reactants' concentration ratio, the progression of the CE process was captured, and tunable crystal phases of the $Cu_{2-x}S$ were achieved. It is proposed that the evolution of $Cu_{2-x}S$ phases in a NW system is dependent on both kinetic and thermodynamic factors. The reported data demonstrate that CE can be used to precisely control

the structure, composition, and crystal phases of NWs, and such control may be generalized to other material systems for a variety of practical applications.
Nanomaterials have attracted much interest and gained widespread use in catalytic,(1) photovoltaic,(2) electronic,(3) and photonic applications(4) because of their interesting mechanical, electrical, and optical properties. In particular, many of these properties sensitively depend on the crystal phases and compositions of the materials. The demand to prepare compositionally diverse, morphologically well-defined nanomaterials with controlled crystal phases is a general challenge that drives the exploration of new synthetic approaches.
In addition to direct synthetic schemes, postsynthetic methods, such as CE,(5-7) are able to yield materials with unprecedented structural and compositional complexity. CE reactions substitute cations within the relatively rigid anion host lattice, utilizing the orders of magnitude difference in diffusivity of cations compared to anions to modify the composition of the template while preserving its morphology. While CE is an age-old phenomenon commonly observed in mineral replacement reactions,(8) its application in the synthesis of bulk materials is limited because of the sluggish diffusion kinetics of cations over large length scales. In contrast, CE reactions work well for the synthesis of nanomaterials owing to the short distance that cations need to travel within the material. In recent years, CE has undergone a revival and has been used to synthesize a variety of advanced nanostructures, including nanomaterials of metastable phases,(9) nanoscale heterostructures,(10) and alloyed nanomaterials.(11)
Metal chalcogenides nanomaterials are good candidates for CE reactions because of their significant ionic character and the capability for cations to diffuse into and out of the lattice.(12, 13) Many of the metal chalcogenides, in particular late-transition-metal sulfides, have special properties that arise from their deficiency of cations. The cation-vacancy ordering in these materials gives rise to distinct crystal phases that have similar crystal structures but different material properties, such as in the cases of nickel sulfide, cobalt sulfide, and $Cu_{2-x}S$.(14) Taking $Cu_{2-x}S$ as an example, there are six experimentally identified, low temperature (<100 °C) stable phases: low chalcocite ($Cu_2S$), djurleite ($Cu_{1.97}S$), digenite ($Cu_{1.8}S$), anilite ($Cu_{1.4}S$), roxbyite ($Cu_{1.75}S$), and covellite (CuS). Among them, low chalcocite, djurleite, and roxbyite have similar hexagonal close-packing sulfur sublattices but significantly different material properties; consequently, each phase is preferred for specific applications. As a component in heterojunction solar cells, the low chalcocite phase is known to be advantageous over other phases.(15, 16) On the other hand, the vacancy-doped deficient $Cu_{2-x}S$, such as djurleite, support localized surface plasmon resonances, whose energy can be dynamically tuned by controlling the free carrier density.(17) Therefore, it is apparent that the different properties of these phases lead to their suitability for various applications, reaffirming the importance of fine-tuning the crystal phase of nanomaterials.
CE is a suitable method to control the phases of late-transition-metal

chalcogenides because it preserves the anionic framework when the size of the nanomaterials is sufficiently large (>5–6 nm)(18) and because these materials share a similar anion sublattice among their different phases. In this work, using wurtzite CdS NW as a starting template, CE reaction conditions are finely tuned to rationally control the crystal phases of the resultant $Cu_{2-x}S$. Three different stages of the CE reaction were revealed with detailed characterization: the initial nucleation of $Cu_{2-x}S$ islands at the surface of CdS NWs, the formation of CdS-$Cu_{2-x}S$ core–shell NWs, and the generation of phase-pure $Cu_{2-x}S$ NWs with controlled phases. Such observed phase evolution of the pure $Cu_{2-x}S$ NWs is dependent on both kinetic and thermodynamic factors, and this system can guide the development of the future synthesis of nanomaterials via CE.

CdS NWs were synthesized via a reported solvothermal approach with slight modification.(19) The as-grown single-crystalline CdS NWs have diameters of about 30–40 nm and lengths up to 10 µm, as shown by TEM (Figure S1a) and SEM (Figure S1c) characterization. Figure S1b indicates the single-crystalline wurtzite CdS NWs oriented in the ⟨002⟩ growth direction. These uniform NWs were chosen as the platform for further study of CE because they avoid potential complicating effects caused by nonuniform size or growth direction.

The reaction between CdS NWs and $[MeCN]_4Cu^{I}PF_6$ in methanol solution was chosen as a model system with which to investigate the CE process. Two independent variables were used: the duration of the CE reaction and the $[Cu^{+}]/[Cd^{2+}]$ ratio. The transformation proceeds from discontinuous $Cu_{2-x}S$ islands nucleating at the surface of CdS to partially converted CdS-$Cu_{2-x}S$ core–shell NWs, and eventually to fully converted $Cu_{2-x}S$ NWs whose phases progress from roxbyite to djurleite and finally to low chalcocite with increasing time and concentration (Figure 1). This controllable evolution demonstrates the capability of CE reactions to synthesize nanomaterials with specific morphologies and crystalline phases. Table S1 details the reaction conditions used to produce the CdS-$Cu_{2-x}S$ and $Cu_{2-x}S$ NWs characterized in this work.

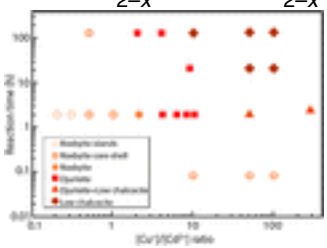

Figure 1. Transformation diagram of CE in the CdS-$Cu_{2-x}S$ system, shows the influence of different parameters on the morphology and phase of the products.

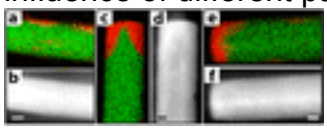

Figure 2. EDS mapping for Cd–L (in green) and Cu–K (in red) and STEM images of CdS–$Cu_{2-x}S$ NWs obtained with a 0.2:1 $[Cu^+]/[Cd^{2+}]$ ratio and 2 h reaction time. (a,b) Conversion at the side facets. (c–f) Conversion at the tips of the NWs. Scale bar, 10 nm.

After introducing a small quantity of $Cu^+$ ions into the CdS NW solution ($[Cu^+]/[Cd^{2+}] \leq 0.3$), discontinuous $Cu_{2-x}S$ islands are formed at the surface of the CdS NWs, as shown in EDS mapping images (Figure 2a). Interestingly, the tips have a thicker layer of conversion than that of the side facets (Figure 2c–f). A similar observation was also reported in the CE of other CdS nanomaterials.(20, 21) It was proposed that the lower formation energy of the CdS–$Cu_{2-x}S$ interface at the end {001} facets, as compared to that of the side facets such as {100}, contributes to the observed phenomenon,(20, 21) although other factors such as the inhomogeneity of surfactant passivation at different facets may also play a role.

Upon applying a higher but still substoichiometric concentration of $Cu^+$ ions ($0.5 \leq [Cu^+]/[Cd^{2+}] < 2$) or a short reaction time (less than 30 min), partially converted samples with core–shell structures were observed (Figure 3a). The XRD spectrum shows a combination of diffraction peaks from both CdS and roxbyite (Figure S2), and the HRTEM image in Figure 3a shows that the CdS core maintains the wurtzite structure with a thin roxbyite shell grown epitaxially at the surface. The small lattice mismatch between $Cu_{2-x}S$ and wurtzite CdS (Tables S2–S5, Figure S3) allows the epitaxial growth of roxbyite shell at the surface of CdS with minimal formation of structural defects.

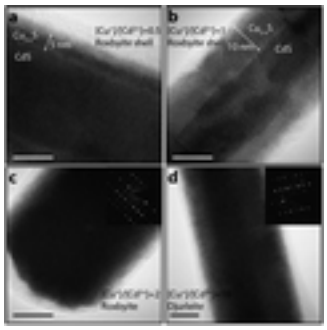

Figure 3. HRTEM images of (a, b) CdS–$Cu_{2-x}S$ core–shell NWs and (c, d) fully converted $Cu_{2-x}S$ NWs with different $[Cu^+]/[Cd^{2+}]$ ratios and a 2 h reaction time. HRTEM image of (a) a core–shell NW obtained with a 0.5:1 $[Cu^+]/[Cd^{2+}]$ ratio, (b) a core–shell NW with increasing shell thickness obtained with a 1:1 $[Cu^+]/[Cd^{2+}]$ ratio, (c) a fully converted roxbyite NW obtained with a 2:1 $[Cu^+]/[Cd^{2+}]$ ratio, and (d) a djurleite NW obtained with a 10:1 $[Cu^+]/[Cd^{2+}]$ ratio. Scale bar, 10 nm.

With an increased $[Cu^+]/[Cd^{2+}]$ ratio (Figure 3) or reaction time (Figure S5), an

increasing degree of CE was observed. At first, a larger $[Cu^{+}]/[Cd^{2+}]$ ratio leads to a thicker $Cu_{2-x}S$ shell (Figure 3a–b). Higher ratios result in fully converted $Cu_{2-x}S$ NWs that evolve from the roxbyite to djurleite phase (Figure 3c–d). Meanwhile, the morphology of the NWs was preserved after CE reaction under different reaction conditions (Figure S4), demonstrating the anionic framework is rigid and unchanged during the reaction. Figure S5 shows the XRD patterns of the $Cu_{2-x}S$ NWs after different durations of CE, illustrating that a longer reaction time leads to the formation of more stoichiometric phases of $Cu_{2-x}S$.

Even though the sulfur sublattice is preserved, the resultant $Cu_{2-x}S$ shell and fully converted $Cu_{2-x}S$ NWs are not single-crystalline but composed of multiple crystalline domains with orientations related by 120° rotations about the hexagonal *c* axis (Figure 4). The djurleite phase was investigated for a more detailed analysis. Table S2 lists structural data for $Cu_{2-x}S$(22) and wurtzite CdS.(20) Traditionally djurleite has been treated as orthorhombic since β is close to 90°, where the unit cell's dimensions (*a*, *b*, *c*) are closely related to those of the hexagonal high chalcocite subcell ($a_h$, $c_h$) with $a = 4a_h$, $b = 4a_h$, $c = 2\sqrt{3}a_h$ (Figure 4b). Since djurleite's unit cell is a simple superstructure of the hcp subcell, it gives rise to three possible orientations of the orthorhombic forms relative to the hcp subcell, which are related by 120° rotations about the hexagonal *c* axis (Figure 4c). It is proposed that at the initial stage of the CE, $Cu_{2-x}S$ islands nucleate at different sites at the surface of the CdS NWs with independent orientations and then merge to form a continuous $Cu_{2-x}S$ shell or fully converted $Cu_{2-x}S$ NWs with large crystalline domains that are rotated by 120° (Figures 3b, 4d–e). This process may be generalized to other CE systems, and it could be one of the underlying reasons for the formation of many of the domains and stacking faults observed in those systems.(6)

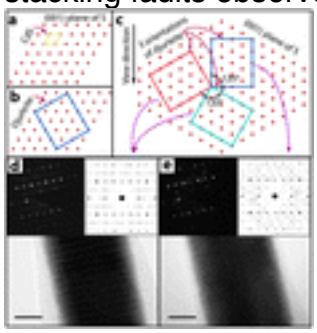

Figure 4. Relation between djurleite's unit cell and the hcp sulfur sublattice. (a, b) CdS and djurleite unit cell relative to the hcp sulfur sublattice. (c) The top direct lattice illustrations show three possible orientations of the djurleite structure relative to the hcp sulfur sublattice. (d, e) HRTEM images of two different segments taken from one NW show djurleite patterns of different orientations, with a zone axis of [012] or $[01\bar{2}]$ for left, [010] for right. Scale bar, 10 nm. Inset:

comparison of the simulated and experimental electron diffraction patterns.
The transformation of CdS NWs into roxbyite, djurleite, and low chalcocite $Cu_{2-x}S$ NWs occurs in a continuous manner with increasing reaction time and $[Cu^{+}]/[Cd^{2+}]$ ratio. Thermodynamically, a previous study by Potter(23) has measured that the standard free energies of formation for different $Cu_{2-x}S$ phases are in favor of higher stoichiometry, but they are fairly close to each other (no more than about $2kT$). These data are consistent with the observation that different phases of $Cu_{2-x}S$ can be synthesized in NWs with slightly different reaction conditions. However, such a conclusion may require further investigation, not only because of the absence of thermodynamic data for roxbyite but also because the measured thermodynamic data are highly sensitive to the presence of oxygen.(23, 24)
The different observations of CE with bulk,(25) NWs, and nanorods(20) of CdS imply an interplay between thermodynamics and kinetics. For CE in CdS thin films, solid-state diffusion is the rate-limiting process.(25) The thickness and stoichiometry of the converted $Cu_{2-x}S$ layers are controlled by Fick's law, which includes factors such as reaction time, temperature, and $Cu^{+}$ ion concentration. In contrast for CE in CdS nanorods,(20) the reaction is mostly controlled by thermodynamics because of its small size; subsequently the reaction yields a low chalcocite phase, the most thermodynamically favored one under oxygen-free conditions.(23) NW behavior is intermediate between that of the nanorods and thin films; it is proposed that both kinetics and thermodynamics should be considered for the structure and phase of the products, owing to the intermediate size of NWs. Additionally since the NW geometry requires longer diffusion paths for the cations, the reaction needs a longer time to reach equilibrium. A further understanding of the thermodynamics and kinetics of the phase evolution phenomenon in the CE reaction will require more experimental and theoretical work, including using isothermal titration calorimetry to follow the energetics of the CE reaction, and conducting simulations to study the solid-state diffusion process.
In conclusion, CE chemistry has been used to transform CdS NWs into phase-controlled $Cu_{2-x}S$ NWs. The overall process occurs in three stages: formation of discontinuous $Cu_{2-x}S$ islands, formation of core–shell CdS–$Cu_{2-x}S$ heterostructures, and complete conversion to $Cu_{2-x}S$ NWs with controllable crystal phases. Detailed structural characterization reveals that the resultant $Cu_{2-x}S$ phases become more stoichiometric with increasing reaction time and copper precursor concentration. Such behavior is intermediate between the behavior of CE observed in nanorods and thin films. This result offers a new avenue to create chemically and compositionally diverse nanomaterials with controlled crystal phases that can be tailored for specific applications.
## Supporting Information

Experimental details, additional TEM, XRD data, and crystal structure information on the reactants and products. This material is available free of charge via the Internet at http://pubs.acs.org.
The authors declare no competing financial interest.
•

## Acknowledgment

This work was supported by the Director, Office of Science, Office of Basic Energy Sciences, Materials Science and Engineering Division, U.S. Department of Energy under Contract No. DE-AC02-05CH11231(P-Chem).
• Reference QuickView
•

## References

This article references 25 other publications.

1. Chen, C.; Kang, Y.; Huo, Z.; Zhu, Z.; Huang, W.; Xin, H. L.; Snyder, J. D.; Li, D.; Herron, J. A.; Mavrikakis, M.; Chi, M.; More, K. L.; Li, Y.; Markovic, N. M.; Somorjai, G. A.; Yang, P.; Stamenkovic, V. R. *Science* **2014**, 343, 1339[CrossRef], [PubMed], [CAS]
2. Rath, A. K.; Bernechea, M.; Martinez, L.; de Arquer, F. P. G.; Osmond, J.; Konstantatos, G. *Nat. Photon* **2012**, 6, 529[CrossRef], [CAS]
3. Lieber, C. M.; Wang, Z. L. *MRS Bull.* **2007**, 32, 99[CrossRef], [CAS]
4. Law, M.; Sirbuly, D. J.; Johnson, J. C.; Goldberger, J.; Saykally, R. J.; Yang, P. *Science* **2004**, 305, 1269[CrossRef], [PubMed], [CAS]
5. Robinson, R. D.; Sadtler, B.; Demchenko, D. O.; Erdonmez, C. K.; Wang, L.-W.; Alivisatos, A. P. *Science* **2007**, 317, 355[CrossRef], [PubMed], [CAS]
6. Zhang, B.; Jung, Y.; Chung, H. S.; Van Vugt, L.; Agarwal, R. *Nano Lett.* **2010**, 10, 149[ACS Full Text], [PubMed], [CAS]
7. Casavola, M.; van Huis, M. A.; Bals, S.; Lambert, K.; Hens, Z.; Vanmaekelbergh, D. *Chem. Mater.* **2012**, 24, 294[ACS Full Text], [CAS]
8. Jenny, H. *J. Phys. Chem.* **1931**, 36, 2217[ACS Full Text]
9. Li, H.; Zanella, M.; Genovese, A.; Povia, M.; Falqui, A.; Giannini, C.; Manna, L. *Nano Lett.* **2011**, 11, 4964[ACS Full Text], [PubMed], [CAS]
10. Demchenko, D. O.; Robinson, R. D.; Sadtler, B.; Erdonmez, C. K.; Alivisatos, A. P.; Wang, L.-W. *ACS Nano* **2008**, 2, 627[ACS Full Text], [PubMed], [CAS]
11. Beberwyck, B. J.; Surendranath, Y.; Alivisatos, A. P. *J. Phys. Chem. C* **2013**, 117, 19759[ACS Full Text], [CAS]
12. Beberwyck, B. J.; Alivisatos, A. P. *J. Am. Chem. Soc.* **2012**, 134, 19977ACS Full Text, [PubMed], [CAS]
13. Son, D. H.; Hughes, S. M.; Yin, Y.; Paul Alivisatos, A. *Science* **2004**, 306, 1009[CrossRef], [PubMed], [CAS]
14. Rao, C. N. R.; Pisharody, K. P. R. *Prog. Solid State Chem.* **1976**, 10 (

Part 4) 207[CrossRef]
15. Reynolds, D. C.; Leies, G.; Antes, L. L.; Marburger, R. E. *Phys. Rev.* **1954**, 96, 533[CrossRef], [CAS]
16. Bragagnolo, J. A.; Barnett, A. M.; Phillips, J. E.; Hall, R. B.; Rothwarf, A.; Meakin, J. D. *IEEE Trans. Electron Devices* **1980**, 27, 645[CrossRef]
17. Luther, J. M.; Jain, P. K.; Ewers, T.; Alivisatos, A. P. *Nat. Mater.* **2011**, 10, 361[CrossRef], [PubMed], [CAS]
18. Jain, P. K.; Amirav, L.; Aloni, S.; Alivisatos, A. P. *J. Am. Chem. Soc.* **2010**, 132, 9997ACS Full Text, [PubMed], [CAS]
19. Yan, P.; Xie, Y.; Qian, Y.; Liu, X. *Chem. Commun.* **1999**, 1293[CrossRef], [CAS]
20. Sadtler, B.; Demchenko, D. O.; Zheng, H.; Hughes, S. M.; Merkle, M. G.; Dahmen, U.; Wang, L.-W.; Alivisatos, A. P. *J. Am. Chem. Soc.* **2009**, 131, 5285ACS Full Text, [PubMed], [CAS]
21. Miszta, K.; Dorfs, D.; Genovese, A.; Kim, M. R.; Manna, L. *ACS Nano* **2011**, 5, 7176[ACS Full Text], [PubMed], [CAS]
22. Putnis, A. *Am. Mineral.* **1977**, 62, 107[CAS]
23. Potter, R. W. *Econ. Geol.* **1977**, 72, 1524[CrossRef], [CAS]
24. Wagman, D. D.; Evans, W. H.; Parker, V. B.; Schumm, R. H.; Halow, I.; Bailey, S. M.; Churney, K. L.; Nuttall, R. L. *J. Phys. Chem. Ref. Data* **1989**, 18, 1807[CrossRef]
25. Salkalachen, S.; Jatar, S.; Rastogi, A. C.; Bhide, V. G. *Sol. Cells* **1981**, 3, 341[CrossRef], [CAS]